ACCOUNTS
of chemical research

Infrared Optical Activity: Electric Field Approaches in Time Domain

HANJU RHEE,[†,‡] JUN-HO CHOI,[§] AND MINHAENG CHO*[,†,§]

[†]*Korea Basic Science Institute, Seoul 136-713, Korea,* [‡]*Graduate School of Analytical Science and Technology, Chungnam National University, Daejeon 305-764, Korea,* [§]*Department of Chemistry, Korea University, Seoul 136-701, Korea*

RECEIVED ON JUNE 22, 2010

CONSPECTUS

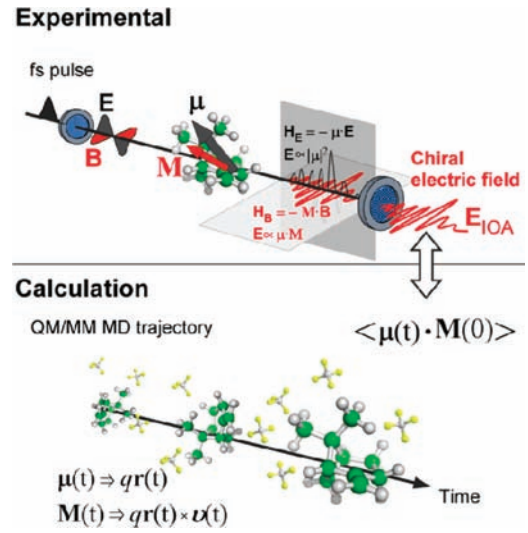

Vibrational circular dichroism (VCD) spectroscopy provides detailed information about the absolute configurations of chiral molecules including biomolecules and synthetic drugs. This method is the infrared (IR) analogue of the more popular electronic CD spectroscopy that uses the ultraviolet and visible ranges of the electromagnetic spectrum. Because conventional electronic CD spectroscopy measures the difference in signal intensity, problems such as weak signal and low time-resolution can limit its utility. To overcome the difficulties associated with that approach, we have recently developed femtosecond IR optical activity (IOA) spectrometry, which directly measures the IOA free-induction-decay (FID), the impulsive chiroptical IR response that occurs over time.

In this Account, we review the time-domain electric field measurement and calculation methods used to simultaneously characterize VCD and related vibrational optical rotatory dispersion (VORD) spectra. Although conventional methods measure the electric field intensity, this vibrational technique is based on a direct phase-and-amplitude measurement of the electric field of the chiroptical signal over time. This method uses a cross-polarization analyzer to carry out heterodyned spectral interferometry. The cross-polarization scheme enables us to selectively remove the achiral background signal, which is the dominant noise component present in differential intensity measurement techniques. Because we can detect the IOA FID signal in a phase-amplitude-sensitive manner, we can directly characterize the time-dependent electric dipole/magnetic dipole response function and the complex chiral susceptibility that contain information about the angular oscillations of charged particles. These parameters yield information about the VCD and VORD spectra.

In parallel with such experimental developments, we have also calculated the IOA FID signal and the resulting VCD spectrum. These simulations use a quantum mechanical/molecular mechanical molecular dynamics (QM/MM MD) method and calculate the electric dipole/magnetic dipole cross-correlation function in the time domain. Although many quantum chemistry calculation approaches can only consider a limited number of geometry-optimized conformations of chiral molecules in a gas phase, this computational method includes the solute−solvent interactions and the inhomogeneous distributions of solute conformers in condensed phases. A subsequent Fourier transformation of the chiral response function produced a theoretical VCD spectrum in the entire mid-IR frequency range.

Directly comparing theory and experiment, we demonstrate quantitative agreement between frequency-tunable femtosecond IOA measurements and QM/MM MD simulations of (1*S*)-β- pinene in CCl_4 solution. We anticipate that these direct IOA measurement and calculation methods will be applied to the studies of equilibrium chiroptical properties and structure determinations. These methods provide tools to investigate ultrafast structural dynamics of chiral systems with unprecedented time resolution.

Published on the Web 10/08/2010 www.pubs.acs.org/acr
10.1021/ar100090q

Introduction

A fundamental difference between quantum mechanical and classical mechanical descriptions of particle dynamics is the phase factor of quantum mechanical wave function.[1] Such phase information is lost when the absolute square of wave function is experimentally measured. Similarly, a free-induction-decay (FID) field **E** generated by the linear polarization of a given material interacting with an incident radiation is a complex function containing an additional time- and space-dependent phase factor exp ($i\phi$) compared to the incident electric field.[2] Conventional circular dichroism is usually based on an intensity measurement technique so that the intensities $|\mathbf{E}|^2$ of the transmitted fields when a chiral solution sample interacts with left- and right-circularly polarized radiations are separately measured. The imaginary part of the additional phase factor is responsible for the differential absorbance of chiral molecules for left- and right-circularly polarized radiations, whereas its real part is associated with the optical rotation of an incident linearly polarized radiation.[3] Direct characterization of such a complex phase factor thus requires special measurement and calculation methods. Recently, it was shown that a combination of cross-polarization analyzer and heterodyned interferometric detection method is capable of measuring both the phase and the amplitude of the IR optical activity (IOA) FID field **E** instead of $|\mathbf{E}|^2$.[4−8] We shall refer to these measurement and calculation methods as electric field approaches.

An IR optical activity extensively studied over the decades is the vibrational circular dichroism (VCD) spectroscopy probing differential interactions of chiral molecules with left- and right-handed chiral IR fields.[9] It was shown to be extremely useful for the studies and determinations of chiral molecule structures and their absolute configurations in condensed phases.[2,10−19] Nevertheless, the conventional methods in experiment and computation still pose their own limitations so that further methodological advancement should be achieved for a wide range of applications including time-resolved VCD studies of biomolecules. To understand this difficulty, it is noted that the vibrational response of a chiral molecule can be approximately described as helical oscillations of charged particles that are associated with nuclear motions in a given chiral molecule. Such helical oscillations can be decomposed into angular and linear components representing chiral and achiral effects, respectively. A major difficulty of the conventional differential absorbance (ΔA) measurement technique is associated with the fact that such angular components (magnetic dipole responses) of the nuclear motions are extremely small in comparison to the linear components (electric dipole responses). Consequently, the VCD (ΔA) signal can be masked by the strong achiral IR absorption signal ($\Delta A/A = 10^{-4}\sim10^{-6}$). In the case of using an intense laser light whose intensity level is much higher than that of a thermal background noise, a huge fluctuating achiral signal (A) becomes the dominant noise factor for measuring the differential absorption ΔA. However, it has been shown that the electric field measurement[4−7] and calculation[20,21] methods based on a time-domain characterization of IOA are alternative and promising approaches overcoming a variety of problems hampering the differential intensity measurement and gas-phase ab initio calculation methods, respectively.

The governing principles of the present electric field measurement method can be understood from an explanation of the non-differential amplitude-level detection scheme, where the IOA field is isolated from the achiral background field and its handedness (phase) and magnitude are characterized. The emitted electric field from the cross-polarization (CP) analyzer accounts for the chirospecific IR response of chiral solution sample and forms a wave packet of IOA FID field carrying complete IOA (VCD and VORD) information over the whole frequency range of the incident IR pulse. Second, direct phase-and-amplitude measurement of the IOA FID field can be achieved by employing a Fourier-transform spectral interferometry (FTSI),[22−27] which is a useful method for characterizing unknown weak electric fields in terms of its spectral phase and amplitude with respect to a reference field called local oscillator and has been widely used in heterodyne-detected two-dimensional (2D) photon echo spectroscopy.[24−26,28] Such heterodyned detection of the IOA FID using a Mach−Zehnder interferometer, where a time delay between the signal and a local oscillator is controllable, provides both VCD and VORD spectra that are imaginary and real parts of the complex chiral susceptibility, $\Delta\chi(\omega)$, respectively.

However, even with the experimentally measured VCD spectrum, often a complete determination of absolute configuration (or multiple configurations) of chiral molecules in solution additionally requires extensive quantum chemistry calculations and comparisons with experimental data, if the solute molecules have a conformation distribution and/or if the structure of an isolated molecule in a gas phase significantly differs from those in solutions. Despite that such an ab initio calculation approach and vibrational exciton coupling models[20,29] have been found to be of effective use, they can provide IOA information on one or just a few selected geometry-optimized conformations of chiral molecules. Consequently, the conformational inhomogeneity and dynamic

solute−solvent interaction effects on VCD spectrum, which are inherently present in chiral molecule solutions, have not been taken into account with ease. In this respect, there have been several theoretical attempts to directly obtain the IR and VCD spectra of chiral molecules in solution using molecular dynamics simulation and time correlation function approach.[30−32] Recently, we employed the so-called quantum mechanical/molecular mechanical molecular dynamics (QM/MM MD) simulation method to simulate the IR and VCD spectra of peptides and chiral molecules in solution.[21,33] It was shown that the time-correlation function approach provides quantitatively reliable results, where the corresponding spectra were obtained by Fourier-transforming the auto- and cross-correlation functions of the electric and magnetic dipole moments calculated from the QM/MM MD trajectories. This time-correlation function approach utilizing entire MD trajectories has certain advantages, because the conformation distribution of chiral molecules such as peptides and the solvation-induced effects on the corresponding spectra are automatically taken into account. In this review, we present simulation results on (1*S*)-β-pinene/CCl_4 solution by carrying out QM/MM MD simulations with the HF/3-21G method for the QM treatment of the solute (1*S*)-β-pinene. The IOA FID fields associated with C−C stretch, C−H bend, C=C stretch, and C−H stretch VCD bands are obtained and compared with experimentally measured IOA FID fields using a femtosecond IR spectral interferometry in time domain. The agreements were found to be acceptable. We shall also present a discussion on the relationships between the femtosecond IOA measurement method and the heterodyne-detected 2D photon echo method as well as between the quasi-null geometry-based ellipsometry of CD and ORD measurement method and the self-heterodyne-detected 2D pump−probe method.

Electric Field Measurement

Phenomenological Description of IOA FID. The IOA FID field containing information on the molecular chirality can be selectively allowed to pass through the cross-polarization analyzer, where a chiral solution sample is placed in between the two crossed linear polarizers (see Figure 1a). When a linearly polarized light after the first linear polarizer passes through the chiral medium, due to the electric field/electric dipole and magnetic field/magnetic dipole interactions, its polarization state is transformed into rotated elliptically polarized light. Here, the circular dichroic ($\Delta\kappa$) and circular birefringent (Δn) effects are combined to contribute to such a polarization state change by chiral molecules. The incident linearly polarized radiation is a 50:50 linear combination of left- and right-circularly polarized (LCP and RCP) radiations. Due to the circular dichroism, the linearly polarized radiation becomes elliptically polarized after the chiral solution sample because the ratio of the LCP to RCP components of the transmitted radiation deviates from a unity. Second, the circular birefringence effect induces specific rotation of the major axis of the transmitted elliptically polarized radiation. In principle, the handedness, ellipticity, and rotation angle of the resultant polarization are completely determined by the linear optical activity property called vibrational rotational strength of the target chiral molecule. In fact, such chiroptical properties result from the relative phase shift and amplitude change of the IOA FID field transmitted through the second linear polarizer whose optic axis is precisely perpendicular to that of the first one (see Figure 1a). On the other hand, the parallel polarization component of which polarization direction is parallel to the optic axis of the first linear polarizer corresponds to the

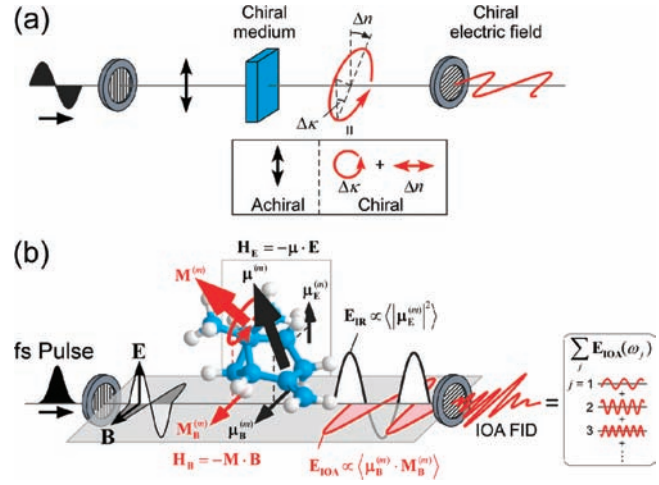

FIGURE 1. Cross-polarization scheme for femtosecond IR optical activity free-induction-decay field measurement. (a) Phenomenological description of the working principle of the cross-polarization detection scheme. Differences in absorption coefficients ($\Delta\kappa$) and refractive indexes (Δn) of chiral molecule for left- and right-circularly polarized radiations are associated with circular dichroism and circular birefringence, respectively. Due to these effects, the incident linearly (vertically) polarized beam is transformed into an inclined elliptically polarized beam, whose horizontal component is directly related to the IOA FID field. (b) Radiation−matter interactions and molecular level description of the cross-polarization detection scheme. For simplicity, only the *m*th molecule with a particular orientation is illustrated among randomly oriented molecules. In this figure, $\boldsymbol{\mu}_E^{(m)}$ is the electric dipole vector component along the direction of **E**-vector, whereas $\boldsymbol{\mu}_B^{(m)}$ and $\mathbf{M}_B^{(m)}$ are the electric dipole and magnetic dipole vector components along the direction of **B**-vector. For an ensemble of randomly oriented molecules, their orientation-averaged inner products, $\langle|\boldsymbol{\mu}_E^{(m)}|^2\rangle$ (dipole strength) and $\langle\boldsymbol{\mu}_B^{(m)}\cdot\mathbf{M}_B^{(m)}\rangle$ (rotational strength) are proportional to the IR FID field (E_{IR}) and the IOA FID field (E_{IOA}), respectively. In the case that there exist multiple IOA-active modes, the IOA FID field is given as the superposition of the corresponding fields.

achiral IR FID field. The specially designed cross-polarization analyzer in Figure 1a is therefore of important use to selectively remove such undesired achiral components. This enhanced selectivity of the chiral (IOA FID) field from the large achiral background component is a key to the success of the present cross-polarization scheme shown in Figure 1.

Molecular Level Description of IOA FID Field. Molecular vibrations excited by an incident IR field can have both linear and angular oscillatory components of asymmetrically distributed atomic partial charges in a given chiral molecule. They are the sources of oscillating electric ($\boldsymbol{\mu}$) and magnetic ($\mathbf{M}$) dipole moments, respectively. The magnitudes and relative orientations of $\boldsymbol{\mu}$ and $\mathbf{M}$ determine the oscillator ($|\boldsymbol{\mu}|^2$) and rotational ($\mathrm{Im}[\boldsymbol{\mu}\cdot\mathbf{M}]$) strengths of a given vibrational mode. To understand how these two different dipoles are probed spectroscopically, one should consider the following radiation−matter interaction Hamiltonian[3,34]

$$H_I = H_E + H_B + \cdots = -\boldsymbol{\mu}\cdot\mathbf{E}(\mathbf{r},t) - \mathbf{M}\cdot\mathbf{B}(\mathbf{r},t) + \cdots \quad (1)$$

The first and second terms are the electric dipole/electric field ($\mathbf{E}$) and magnetic dipole/magnetic field ($\mathbf{B}$) interactions, respectively. Figure 1b depicts a schematic representation of the IOA FID field generation. When an impulsive ($\sim$ tens of femtoseconds) IR field that is linearly polarized ($\mathbf{E}$, vertical; $\mathbf{B}$, horizontal) interacts with chiral molecules in solution, the electric and magnetic dipole operators, which are projected components onto the directions of $\mathbf{E}$ and $\mathbf{B}$ vectors, induce vibrational transition and put the interacting solute molecules on vibrational coherences. The time-dependent expectation values of these dipole operators correspond to the linear polarizations that are responsible for the generated IR FID (E_{IR}) and IOA FID (E_{IOA}) fields. For the jth vibrational mode with frequency of ω_j, $E_{\mathrm{IR}}(\omega_j,t)$ and $E_{\mathrm{IOA}}(\omega_j,t)$ can be approximately written as

$$E_{\mathrm{IR}}(\omega_j,t) \propto \langle|\boldsymbol{\mu}_{j,E}^{(m)}|^2\rangle \exp(i\omega_j t)\, f_j(t) = \frac{1}{3}|\boldsymbol{\mu}_j^{(m)}|^2 \exp(i\omega_j t)\, f_j(t) \quad (2)$$

$$E_{IOA}(\omega_j,t) \propto \langle\boldsymbol{\mu}_{j,B}^{(m)}\cdot\mathbf{M}_{j,B}^{(m)}\rangle \exp(i\omega_j t) f_j(t) = \frac{1}{3}[\boldsymbol{\mu}_j^{(m)}\cdot\mathbf{M}_j^{(m)}] \exp(i\omega_j t) f_j(t) \quad (3)$$

where $\boldsymbol{\mu}_j^{(m)}$ and $\mathbf{M}_j^{(m)}$ are the transition electric and magnetic dipole moments of the jth vibrational mode of the mth molecule and the subscripts, E and B, denote their vector components that are parallel to the unit vectors of $\mathbf{E}$ and $\mathbf{B}$, respectively. Here, $\langle\cdots\rangle$ means the rotational averaging over randomly oriented chiral molecules, and $f_j(t)$ is the relaxation function describing vibrational dephasing effects on the IR and IOA spectra. Since the transmission axis of the analyzer (the second linear polarizer in Figure 1b) is parallel to the magnetic field vector $\mathbf{B}$ not $\mathbf{E}$, only the IOA FID field, $E_{\mathrm{IOA}}(\omega_j,t)$, selectively transmits through the analyzer. In contrast, the IR FID field $E_{\mathrm{IR}}(\omega_j,t)$ whose direction is perpendicular to the optic axis of the second linear polarizer is completely rejected if the linear polarizer is perfect. The relative phase and amplitude of $E_{\mathrm{IOA}}(\omega_j,t)$ compared to the incident IR field are determined by the orientation-averaged inner product of $\boldsymbol{\mu}_{j,B}^{(m)}$ and $\mathbf{M}_{j,B}^{(m)}$ (laboratory frame), that is, $\langle\boldsymbol{\mu}_{j,B}^{(m)}\cdot\mathbf{M}_{j,B}^{(m)}\rangle$, which is by definition proportional to the rotational strength, $\mathrm{Im}[\boldsymbol{\mu}_j^{(m)}\cdot\mathbf{M}_j^{(m)}]$ (molecular frame). For a collection of IOA-active modes, the IOA FID field, which can be viewed as a chiral wave packet, is then given as a superposition of all the contributing fields, that is, $E_{\mathrm{IOA}}(t) = \sum_j E_{\mathrm{IOA}}(\omega_j,t)$ (see Figure 1b).

Phase-and-Amplitude Measurement of the IOA FID. Although the IOA FID field transmitted through the cross-polarization analyzer contains entire linear optical activity information, it is in fact coupled to the IR FID component E_{IR} via the Maxwell equation. According to our theory discussed in ref 4, the IOA FID spectrum is linearly proportional to the IR FID spectrum and the proportionality factor is the frequency-dependent chiral susceptibility, $\Delta\chi(\omega)$, that is,

$$\Delta\chi(\omega) \propto \left(\frac{n(\omega)c}{\omega L}\right)\frac{E_{\mathrm{IOA}}(\omega)}{E_{\mathrm{IR}}(\omega)} \quad (4)$$

where $n(\omega)$, c, and L are the refractive index, speed of light, and path length of the sample cell, respectively. The above result eq 4 suggests that measuring both $E_{\mathrm{IOA}}(\omega)$ and $E_{\mathrm{IR}}(\omega)$ spectra yields $\Delta\chi(\omega)$.

It is Fourier-transform spectral interferometry (FTSI) that was used to measure $E_{\mathrm{IOA}}(\omega)$ and $E_{\mathrm{IR}}(\omega)$ spectra. Figure 2a depicts a schematic representation of the heterodyned IOA/IR FID detection setup using Mach−Zehnder interferometry. The FTSI method first measures the heterodyned spectral interferogram resulting from an interference between the FID field either E_{IOA} or E_{IR} and a strong local oscillator field (E_{LO}), where the delay time τ_{D} between the two pulsed fields is fixed. Particularly, the IOA/IR FID spectral interferograms denoted as $S_{\mathrm{IOA,IR}}(\omega)$ are recorded using a properly chosen array detector, where $S_{\mathrm{IOA,IR}}(\omega)$ is given as

$$S_{\mathrm{IOA,IR}}(\omega) = 2\mathrm{Re}[E_{\mathrm{IOA,IR}}(\omega)E_{\mathrm{LO}}^{*}(\omega)\exp(i\omega\tau_{\mathrm{D}})] \quad (5)$$

Figure 2b explains the standard Fourier and inverse Fourier transform procedure that was used to retrieve the VCD and VORD spectra from the experimentally measured $S_{\mathrm{IOA,IR}}(\omega)$ that are real functions of frequency. Not only because the $\Delta\chi(\omega)$ is proportional to the ratio of $E_{\mathrm{IOA}}(\omega)$ to $E_{\mathrm{IR}}(\omega)$ (eq 4) but also because the phase contribution from the reference term

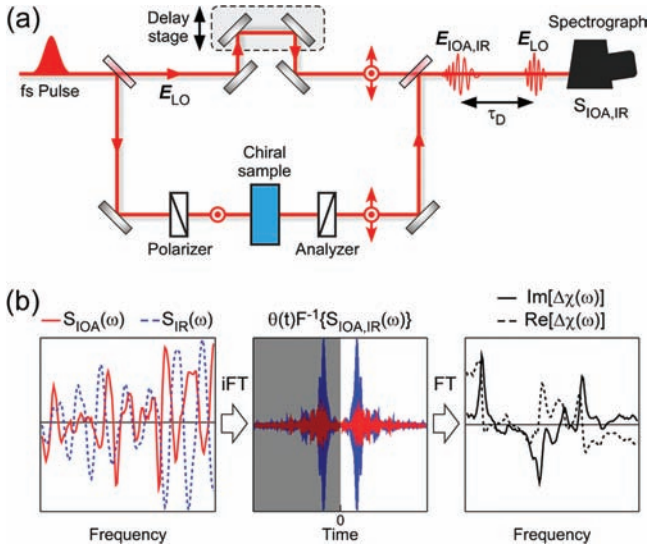

FIGURE 2. (a) Heterodyned spectral interferometric measurement setup of the IR (E_{IR}) and IOA FID (E_{IOA}) fields. A modified Mach−Zehnder interferometer (for active-heterodyning) is used. (b) Stepwise FTSI procedure for obtaining the VCD and VORD spectra from the experimentally measured spectral interferograms, $S_{IR,IOA}(\omega)$ with the setup shown in (a). Step 1: the spectral interferograms $S_{IR,IOA}(\omega)$ in frequency domain are measured. Step 2: the positive part of the inverse Fourier transform of $S_{IR,IOA}(\omega)$ is taken. Step 3: Fourier transformation of thus obtained time-domain profile is performed. Step 4: $\Delta\chi(\omega)$ is obtained by taking the ratio of the IOA FID spectrum to the IR FID spectrum (see eqs 4−6).

$E^*_{LO}(\omega)\exp(i\omega\tau_D)$ cancels out while taking the ratio, the chiral susceptibility spectrum can be obtained in a straightforward manner as

$$\Delta\chi(\omega) \propto E_{IOA}(\omega)/E_{IR}(\omega) \propto F\left[\theta(t)F^{-1}\{S_{IOA}(\omega)\}\right]/F\left[\theta(t)F^{-1}\{S_{IR}(\omega)\}\right] \quad (6)$$

where $F(\cdots)$ and $F^{-1}(\cdots)$ denote the Fourier and inverse Fourier transformations, respectively, and $\theta(t)$ is the Heavyside step function. The relationship in eq 6 is the working formula that has been used to convert the experimentally measured spectral interferograms into the complex susceptibility.

Analogy between IOA FID Measurement and Two-Dimensional Photon Echo. Despite that the present technique uses an active heterodyne-detection technique, it should be mentioned that the so-called ellipsometric technique using a quasi-null geometry with two linear polarizers,[2,35,36] which was pioneered by Kliger and co-workers, shares a very similar optical setup. Much like the cross-polarization scheme, two crossed linear polarizers were used. However, instead of a linearly polarized radiation, an elliptically polarized beam with a vertical major axis was used to generate an electronic OA FID field in the visible frequency domain. It was then detected by allowing its interference with the residual horizontal component of the incident elliptically polarized beam; note that an elliptically polarized radiation is given as a linear combination of linearly polarized and circularly polarized beams. Even though this technique is still an intensity (not phase-and-amplitude) measurement method, it can be considered to be a self-heterodyne-detection scheme. Recently, Helbing and Bonmarin clearly showed that such an ellipsometric technique can be extended to the IR region to measure the VCD and VORD spectra with a significantly enhanced detection sensitivity.[37] The principal difference between this and ours is how to control the relative phase between signal and reference fields during the heterodyning process. In the ellipsometric detection geometry, the chiral signal field interferes with the incident horizontal electric field itself, which acts as a local oscillator (for self-heterodyning) as well as an excitation field. Thus, the phase delay between the chiral signal and intrinsic local oscillator fields is not experimentally controllable. As a result, the imaginary (VCD) and real (VORD) parts of the IOA response should be measured separately. On the other hand, the present cross-polarization interferometric technique shown in Figure 2a uses an external local oscillator (for active-heterodyning) so that both the imaginary and real parts of $\Delta\chi(\omega)$ can be simultaneously obtained via the FTSI procedure discussed above.

Interestingly, the relationship between these two methods is quite similar to that between self-heterodyne-detected pump−probe with two pulses and active-heterodyne-detected stimulated photon echo with four pulses. The latter two methods have been widely used to measure the 2D optical spectra of biomolecules,[38−40] light-harvesting systems,[25] semiconductors,[26,41,42] chemical exchange systems,[43,44] and so on. Despite that the frequency-resolved pump−probe experiment is comparatively easy to perform, information on the absorptive part of the 2D response spectrum can only be extracted from the signal. In contrast, the heterodyned photon echo techniques can be of use to measure both the absorptive and dispersive parts of the complex 2D response spectrum.

Experimentally Measured VCD and VORD Spectra of (1*S*)-*β*-Pinene. To demonstrate the experimental feasibility of femtosecond IOA FID measurement technique and also to make direct comparisons with theory, we considered (1*S*)-*β*-pinene/CCl_4 solution; note that (1*S*)-*β*-pinene is a standard chiral organic molecule studied before.[45] We shall focus on four distinctively different groups of vibrational modes that are C−C stretch modes (1000−1350 cm^{-1}), a C═C stretch mode (1600−1700 cm^{-1}), C−H bending modes (1400−1500 cm^{-1}), and C−H stretch modes (2850−3000 cm^{-1}). To perform the heterodyned IOA FID measurements, we deliberately

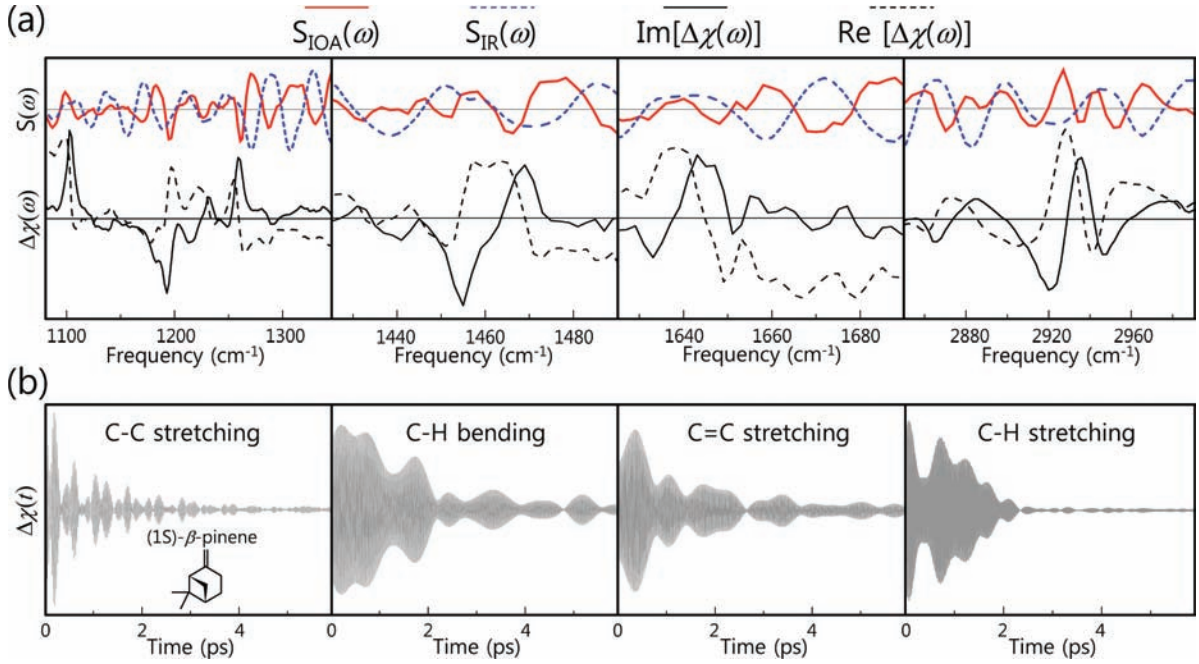

FIGURE 3. (a) Experimentally measured spectral interferograms (upper) by properly tuning the center frequency of the IR pulse spectrum to measure the IOA responses from the C−C stretch (6.6 M), C−H bend (2M), C=C stretch (2M), and C−H stretch (0.3M) vibrations of (1*S*)-β-pinene/CCl_4 solution. The sampling time of the time-domain signal $\theta(t)F^{-1}\{S_{IOA}(\omega)\}$ (middle of Figure 2b, the data are not shown) is set to ~1 fs that is determined by the size of the frequency window ($0-10^{15}$ s^{-1}) taken for the inverse Fourier transformation. The imaginary and real parts of $\Delta\chi(\omega)$ correspond to the VCD and VORD spectra (see the solid and dashed black lines in this figure). It is noted that dichroic calcite polarizers[50] instead of Brewster's angle germanium polarizers were used for the measurements of spectral interferograms of C−H stretching vibrations. Linear baseline corrections were made to obtain the Im[$\Delta\chi(\omega)$] spectra (black solid line) of C−H bending and C−H stretching vibrations (second and fourth from the left). (b) Time-domain IOA response functions, $\Delta\chi(t)$, obtained by Fourier-transforming the experimentally measured $\Delta\chi(\omega)$.

tuned the center frequency (ω_c) of the femtosecond IR pulse whose spectral width is about 200 cm^{-1}. One of the crucial optical elements for the success of the present experiments was Brewster angle germanium polarizers having an extremely small extinction ratio of about 10^{-9} over the broad IR frequency range from 20 to 10 000 cm^{-1}.[7,46] Such a small value of extinction ratio means that one out of 10^9 photons in a vertically polarized incident beam is transmitted through this linear polarizer whose optic axis is horizontally aligned.

In the upper panel of Figure 3a, the experimentally measured spectral interferograms, $S_{IOA}(\omega)$ (red solid lines) and $S_{IR}(\omega)$ (blue dashed lines) of (1*S*)-β-pinene are plotted. The chiral IR susceptibility, $\Delta\chi(\omega)$, is then retrieved from these interferograms using eq 6, and the resultant imaginary (differential absorptive) and real (differential dispersive) parts are plotted in the same figure. The characteristic VCD features of (1*S*)-β-pinene, Im[$\Delta\chi(\omega)$], are consistent with the results obtained by using a FT-IR VCD spectrometer,[45,46] even though the VCD spectrum of the C=C stretch mode (1600−1700 cm^{-1}) appears to be comparatively noisy, which is presumably due to IR absorption by water vapor. This shows that the present phase-sensitive detection technique has advantages over the differential intensity measurement method.

Electric Field Calculation

In the previous section, we presented a discussion on the electric field measurement method and results on (1*S*)-β-pinene solution. For the sake of comparison with theory, we obtained the IOA response function, $\Delta\chi(t)$, by Fourier-transforming the experimentally measured $\Delta\chi(\omega)$; note that the IOA/IR FID field in the time domain was obtained from the corresponding spectral interferograms (see eq 6). Each individual $\Delta\chi(t)$ associated with the four different groups of vibrational modes is plotted in Figure 3b. It was shown that the IOA response function is related to the electric dipole/magnetic dipole cross-correlation function, $\langle \boldsymbol{\mu}(t)\cdot\mathbf{M}(0)\rangle$, which can be directly calculated from the QM/MM MD trajectories.[21,30] It should be emphasized that a fully classical MD simulation treating both solute and solvent molecules with a set of force field parameters does not provide quantitatively reliable results on the transition electric and magnetic dipoles of chiral molecules. This is because (i) the intramolecular harmonic potential functions are not accurate, (ii) partial charge fluctuations induced

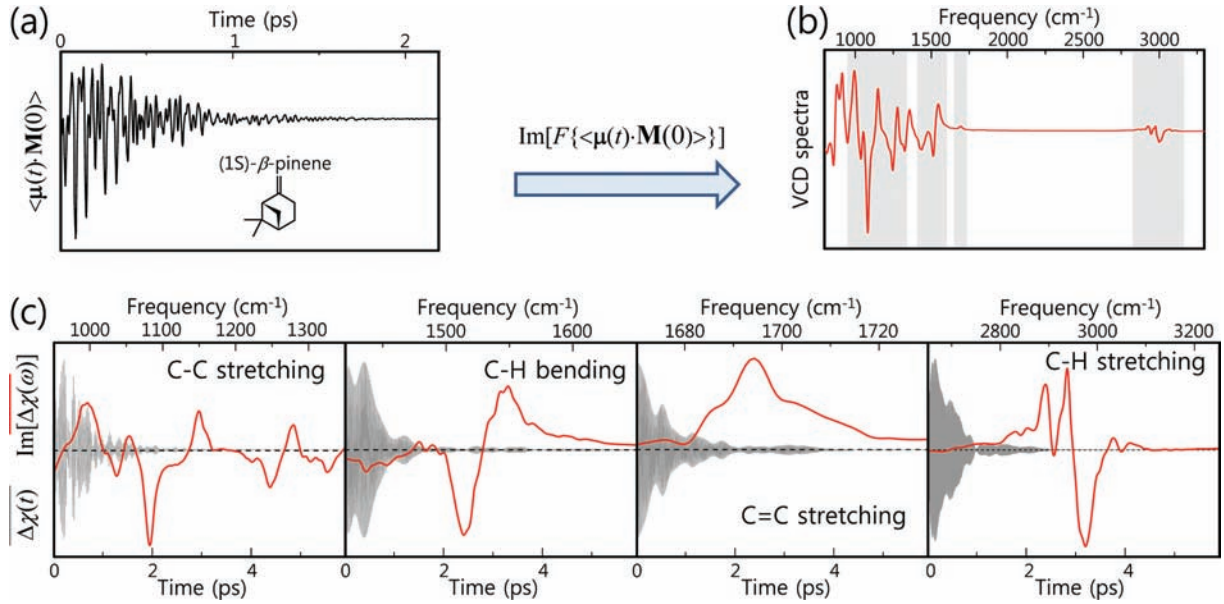

FIGURE 4. (a) Electric dipole/magnetic dipole correlation function, $\langle \boldsymbol{\mu}(t) \cdot \mathbf{M}(0) \rangle$, obtained by using the QM/MM MD trajectories of (1*S*)-β-pinene dissolved in CCl_4 and by treating the nuclear vibrations of this molecule classical mechanically. Its sampling time is 2.5 fs. (b) Imaginary part of the Fourier-transformed spectrum of $\langle \boldsymbol{\mu}(t) \cdot \mathbf{M}(0) \rangle$, which corresponds to the entire VCD spectrum in the frequency range from 800 to 3300 cm^{-1}. (c) Decomposed time-domain IOA response function, $\Delta\chi(t)$, into the four target vibrational modes (gray regions in the full spectrum shown in (b)). Also, the calculated VCD spectra (red lines) are plotted in the four panels of (c).

by solute−solvent interactions are not properly taken into account, and (iii) charge fluxes due to intramolecular vibrations of intrinsically polarizable solute molecule are ignored in the classical MD simulations.

In order to run QM/MM MD simulations of (1*S*)-β-pinene/CCl_4 solution, the solute was treated quantum mechanically with the HF/3-21G method. In total, 186 CCl_4 molecules are treated classical mechanically[47] with the CHARMM force fields.[48] The resultant spherical solvation shell has a radius of about 25 Å, and the solute molecule is placed at the center. To avoid evaporation of solvent molecules at 273 K, a harmonically bound potential is employed. The solute−solvent system was initially energy minimized by using the steepest descent and the adopted basis Newton−Raphson methods. Then, the composite system was heated up to 273 K and equilibrated for 25 ps. The time step used was 0.5 fs, and the total QM/MM MD simulation run time was 300 ps. The coordinates and velocities of the constituent atoms of the (1*S*)-β-pinene molecule were saved for every 2.5 fs time step so that even the high-frequency C−H stretching vibrations were properly described. For the present QM/MM MD simulation studies, we specifically used the CHARMM program interfaced with the GAMESS-UK package.[49]

The electric dipole and magnetic dipole moments of (1*S*)-β-pinene were calculated as

$$\boldsymbol{\mu}(t) = \sum_i q_i(t)\, \mathbf{r}_i(t) \quad \text{and} \quad \mathbf{M}(t) = \frac{1}{2c} \sum_i q_i(t)\, \mathbf{r}_i(t) \times \mathbf{v}_i(t) \quad (7)$$

Here $q_i(t)$, $\mathbf{r}_i(t)$, and $\mathbf{v}_i(t)$ are the Mulliken partial charge, position, and velocity of the *i*th atom. Then, the VCD spectrum $\Delta A(\omega)$ was obtained by taking the imaginary part of the Fourier transform of the electric dipole/magnetic dipole cross-correlation function, that is,

$$\Delta A I(\omega) \propto \mathrm{Im}[\Delta\chi(\omega)] \propto \mathrm{Im} \int_{-\infty}^{\infty} dt\, e^{i\omega t} \langle \boldsymbol{\mu}(t) \cdot \mathbf{M}(0) \rangle \quad (8)$$

The cross correlation function and the VCD spectrum in the frequency range from 800 to 3300 cm^{-1} are plotted in Figure 4a and b, respectively, where the frequency scaling factor of 0.9085 was used.

For direct comparisons with experimental results, the whole VCD spectrum given in Figure 4b is divided into four frequency regions that correspond to the C−C stretch, C−H bend, C=C stretch, and C−H stretch bands (see the red lines in Figure 4c). The time-domain response functions (gray lines in Figure 4c) of each band are obtained by performing a proper inverse Fourier transformation of the corresponding segmented spectrum. To reduce the noise originating from limited lengths of the simulation trajectories, an exponential (apodization) function $\exp(-t/2T_1)$ with $T_1 = 1$ ps (for C−C stretchs, C−H bendings, and C=C stretch) or 300 fs (for C−H stretchs) was multiplied with the time correlation functions.

As can be seen in Figure 4c, the C−H bending mode VCD spectrum exhibits a (−,+) line shape, which is in good agree-

CHART 1. Comparisons between Frequency- (left) and Time-Domain (right) IOA Calculation (upper panels) and Measurement (lower panels) Methods

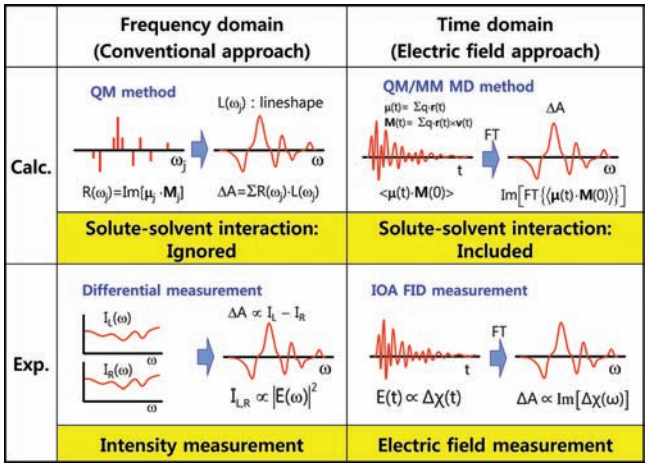

ment with the experimentally measured spectrum shown in Figure 3a. The C=C stretch band appears to be a single positive peak. The peak intensity distribution within the simulated C−H stretch VCD band in Figure 4c does not completely match with the experimental result. Nevertheless, the overall "W"-shape spectral feature originating from complicated interferences among various C−H stretch normal mode IOA fields is successfully reproduced by the simulation. Even with a limited accuracy of the HF/3-21G method used here, it is believed that the overall line shape of the simulated VCD spectrum of (1*S*)-β-pinene/CCl_4 solution (not an isolated (1*S*)-β-pinene molecule) is comparable to the femtosecond IOA FID spectrum. It is expected that a better agreement between the theory and experiment would be found if a combination of density functional theory and high-level basis set is used to run the QM/MM MD simulations, which are still highly expensive. However, we believe that the initial goal of comparing the recently developed electric field measurement and calculation methods for a specific case has been successfully achieved in the present comparative investigations.

Concluding Remarks

The experimental and computational electric field approaches discussed in this Account are briefly summarized in the right panel of Chart 1, where the conventional frequency-domain methods (left panel) are also schematically described together for comparison.

The time correlation function approach utilizing the QM/MM MD trajectory takes into consideration the complicated solute−solvent interactions and overall dynamical events, which were however ignored or crudely described in ab initio calculations of an isolated chiral molecule. Experimentally, the spectral interferometric IOA FID measurement method allows us to directly access the time-domain IOA response function and the corresponding susceptibility giving VCD and VORD spectra simultaneously. The non-differential heterodyned IOA FID field detection scheme enables achiral background-free measurement and offers significantly enhanced selectivity of the chiral signal field. There is a close connection between the two electric field approaches in experiment and theory in that both of them record the electric dipole/magnetic dipole correlation function, $\langle \boldsymbol{\mu}(t) \cdot \mathbf{M}(0) \rangle$. In the present Account, we showed that the experimentally measured IOA spectra of (1*S*)-β-pinene are in agreement with those from electric dipole/magnetic dipole cross-correlation functions.

Up to now, we have discussed the IOA measurements and calculations of chiral molecules in a thermal equilibrium state. However, the same principles also apply to the other vibrational optical activity spectroscopy, which is Raman optical activity. Another potentially interesting application will be studies of biological functions and chemical reactions that are accompanied by structural changes of involved chiral molecules. This will require a high-speed chiroptical measurement technique to monitor the resultant IOA changes in real time. Ultrafast time-resolved IOA spectroscopy will, without a doubt, be an important tool in the future, and such an experiment would be realized by combining a properly designed triggering method that is capable of initiating certain non-equilibrium processes virtually instantaneously. It is believed that the present time-domain electric field approaches will be extremely useful not only in studying the ensemble-average structures of chiral molecules in condense phases but also in understanding a wide range of ultrafast dynamical processes in biology and chemistry of natural chiral biomolecules such as proteins and nucleic acids.

This work was supported by a KBSI grant (T30401) to H.R. and M.C., and by a NRF grant (20090078897) to M.C. We are grateful to Sung-Hyun Ahn for helping us to make all the figures in this paper.

BIOGRAPHICAL INFORMATION

Hanju Rhee received a Ph.D. in 2006 from Pohang University of Science and Technology in Korea under the direction of Prof. Taiha Joo. After 4 years of postdoctoral research in Korea, he has been a senior researcher at Korea Basic Science Institute since 2009 and an adjunct professor in Graduate School of Analytical Science and Technology since 2010.

Jun-Ho Choi received a Ph.D. in 1996 from Seoul National University in Korea under the direction of Sangyoub Lee. He has been working as a research professor at Korea University since 2000.

Minhaeng Cho received a Ph.D. from University of Chicago in 1993 under the direction of Prof. Graham R. Fleming. After 2 years of postdoctoral training at MIT in Prof. Robert J. Silbey's group, he has been on the faculty of Korea University since 1996.

FOOTNOTES

*To whom correspondence should be addressed. E-mail: mcho@korea.ac.kr.

REFERENCES

1 Dirac, P. A. M. *The Principles of Quantum Mechanics*; Oxford University Press: New York, 1958.

2 Berova, N.; Nakanishi, K.; Woody, R. W. *Circular Dichroism: Principles and Applications*; Wiley-VCH: New York, 2000.

3 Cho, M. *Two-Dimensional Optical Spectroscopy*; CRC Press: New York, 2009.

4 Rhee, H.; Ha, J.-H.; Jeon, S.-J.; Cho, M. Femtosecond spectral interferometry of optical activity: theory. *J. Chem. Phys.* **2008**, *129*, 094507.

5 Rhee, H.; June, Y.-G.; Lee, J.-S.; Lee, K.-K.; Ha, J.-H.; Kim, Z. H.; Jeon, S.-J.; Cho, M. Femtosecond characterization of vibrational optical activity of chiral molecules. *Nature* **2009**, *458*, 310–313.

6 Rhee, H.; June, Y.-G.; Kim, Z. H.; Jeon, S.-J.; Cho, M. Phase sensitive detection of vibrational optical activity free-induction-decay: vibrational CD and ORD. *J. Opt. Soc. Am. B* **2009**, *26*, 1008–1017.

7 Rhee, H.; Kim, S.-S.; Jeon, S.-J.; Cho, M. Femtosecond measurements of vibrational circular dichroism and optical rotatory dispersion spectra. *ChemPhysChem* **2009**, *10*, 2209–2211.

8 Vaccaro, P. H. Handedness in quick time. *Nature* **2009**, *458*, 289–290.

9 Nafie, L. A.; Cheng, J. C.; Stephens, P. J. Vibrational circular dichroism of 2,2,2-trifluoro-1-phenylethanol. *J. Am. Chem. Soc.* **1975**, *97*, 3842–3843.

10 Keiderling, T. A. Vibrational CD of biopolymers. *Nature* **1986**, *322*, 851–852.

11 Silva, R. A. G. D.; Kubelka, J.; Bouř, P.; Decatur, S. M.; Keiderling, T. A. Site-specific conformational determination in thermal unfolding studies of helical peptides using vibrational circular dichroism with isotopic substitution. *Proc. Natl. Acad. Sci. U.S.A.* **2000**, *97*, 8318–8323.

12 Freedman, T. B.; Cao, X.; Dukor, R. K.; Nafie, L. A. Absolute configuration determination of chiral molecules in the solution state using vibrational circular dichroism. *Chirality* **2003**, *15*, 743–758.

13 Choi, J.-H.; Cho, M. Amide I vibrational circular dichroism of dipeptide: Conformation dependence and fragment analysis. *J. Chem. Phys.* **2004**, *120*, 4383–4392.

14 Choi, J.-H.; Hahn, S.; Cho, M. Vibrational spectroscopic characteristics of secondary structure polypeptides in liquid water: Constrained MD simulation studies. *Biopolymers* **2006**, *83*, 519–536.

15 Choi, J.-H.; Lee, H.; Lee, K.-K.; Hahn, S.; Cho, M. Computational spectroscopy of ubiquitin: Comparison between theory and experiments. *J. Chem. Phys.* **2007**, *126*, 045102.

16 Lee, K.-K.; Oh, K.-I.; Lee, H.; Joo, C.; Han, H.; Cho, M. Dipeptide structure determination by vibrational circular dichroism combined with quantum chemistry calculations. *ChemPhysChem* **2007**, *8*, 2218–2226.

17 Stephens, P. J.; Devlin, F. J.; Pan, J.-J. The determination of the absolute configurations of chiral molecules using vibrational circular dichroism (VCD) spectroscopy. *Chirality* **2008**, *20*, 643–663.

18 Polavarapu, P. L. *Vibrational Spectra: Principles and Applications with Emphasis on Optical Activity*; Elsevier: Amsterdam, 1998; Vol. 85.

19 Stephens, P. J.; Lowe, M. A. Vibrational circular dichroism. *Annu. Rev. Phys. Chem.* **1985**, *36*, 213–241.

20 Jeon, J.; Yang, S.; Choi, J.-H.; Cho, M. Computational vibrational spectroscopy of peptides and proteins in one and two dimensions. *Acc. Chem. Res.* **2009**, *42*, 1280–1289.

21 Yang, S.; Cho, M. Direct calculations of vibrational absorption and circular dichroism spectra of alanine dipeptide analog in water: Quantum mechanical/molecular mechanical molecular dynamics simulations. *J. Chem. Phys.* **2009**, *131*, 135102.

22 Lepetit, L.; Chériaux, G.; Joffre, M. Linear techniques of phase measurement by femtosecond spectral interferometry for applications in spectroscopy. *J. Opt. Soc. Am. B* **1995**, *12*, 2467–2474.

23 Fittinghoff, D. N.; Bowie, J. L.; Sweetser, J. N.; Jennings, R. T.; Krumbugel, M. A.; DeLong, K. W.; Trebino, R.; Walmsley, I. A. Measurement of the intensity and phase of ultraweak, ultrashort laser pulses. *Opt. Lett.* **1996**, *21*, 884–886.

24 Zanni, M. T.; Ge, N.-H.; Kim, Y. S.; Hochstrasser, R. M. Two-dimensional IR spectroscopy can be designed to eliminate the diagonal peaks and expose only the crosspeaks needed for structure determination. *Proc. Natl. Acad. Sci. U.S.A.* **2001**, *98*, 11265–11270.

25 Brixner, T.; Stenger, J.; Vaswani, H. M.; Cho, M.; Blankenship, R. E.; Fleming, G. R. Two-dimensional spectroscopy of electronic couplings in photosynthesis. *Nature* **2005**, *434*, 625–628.

26 Zhang, T. H.; Borca, C. N.; Li, X.; Cundiff, S. T. Optical two-dimensional Fourier transform spectroscopy with active interferometric stabilization. *Opt. Express* **2005**, *13*, 7432–7441.

27 Lim, S.-H.; Caster, A. G.; Leone, S. R. Fourier transform spectral interferometric coherent anti-Stokes Raman scattering (FTSI-CARS) spectroscopy. *Opt. Lett.* **2007**, *32*, 1332–1334.

28 Khalil, M.; Demirdöven, N.; Tokmakoff, A. Coherent 2D IR spectroscopy: molecular structure and dynamics in solution. *J. Phys. Chem. A* **2003**, *107*, 5258–5279.

29 Krummel, A. T.; Zanni, M. T. Interpreting DNA vibrational circular dichroism spectra using a coupling model from two-dimensional infrared spectroscopy. *J. Phys. Chem. B* **2006**, *110*, 24720–24727.

30 Abbate, S.; Longhi, G.; Kwon, K.; Moscowitz, A. The use of cross-correlation functions in the analysis of circular dichroism spectra. *J. Chem. Phys.* **1998**, *108*, 50–62.

31 Schmitz, M.; Tavan, P. Vibrational spectra from atomic fluctuations in dynamics simulations. II. Solvent-induced frequency fluctuations at femtosecond time resolution. *J. Chem. Phys.* **2004**, *121*, 12247–12258.

32 Horníček, J.; Kaprálová, P.; Bouř, P. Simulations of vibrational spectra from classical trajectories: Calibration with *ab initio* force fields. *J. Chem. Phys.* **2007**, *127*, 084502.

33 Yang, S.; Cho, M. IR spectra of N-methylacetamide in water predicted by combined quantum mechanical/molecular mechanical molecular dynamics simulations. *J. Chem. Phys.* **2005**, *123*, 134503.

34 Loudon, R. *The Quantum Theory of Light*; Oxford University Press: New York, 1983.

35 Lewis, J. W.; Tilton, R. F.; Einterz, C. M.; Milder, S. J.; Kuntz, I. D.; Kliger, D. S. New techniques for measuring circular dichroism changes on a nanosecond time scale. Application to (carbonmonoxy)myoglobin and (carbonmonoxy)hemoglobin. *J. Phys. Chem.* **1985**, *89*, 289–294.

36 Goldbeck, R. A.; Kim-Shapiro, D. B.; Kliger, D. S. Fast natural and magnetic circular dichroism spectroscopy. *Annu. Rev. Phys. Chem.* **1997**, *48*, 453–479.

37 Helbing, J.; Bonmarin, M. Vibrational circular dichroism signal enhancement using self-heterodyning with elliptically polarized laser pulses. *J. Chem. Phys.* **2009**, *131*, 174507.

38 Kolano, C.; Helbing, J.; Kozinski, M.; Sander, W.; Hamm, P. Watching hydrogen dynamics in a beta-turn by transient 2D-IR spectroscopy. *Nature* **2006**, *444*, 469–472.

39 Shim, S.-H.; Gupta, R.; Ling, Y. L.; Strasfeld, D. B.; Raleigh, D. P.; Zanni, M. T. Two-dimensional IR spectroscopy and isotope labeling defines the pathway of amyloid formation with residue-specific resolution. *Proc. Natl. Acad. Sci. U.S.A.* **2009**, *106*, 6614–6619.

40 Demirdöven, N.; Cheatum, C. M.; Chung, H. S.; Khalil, M.; Knoester, J.; Tokmakoff, A. Two-dimensional infrared spectroscopy of antiparallel beta-sheet secondary structure. *J. Am. Chem. Soc.* **2004**, *126*, 7981–7990.

41 Stone, K. W.; Gundogdu, K.; Turner, D. B.; Li, X.; Cundiff, S. T.; Nelson, K. A. Two-quantum 2D FT electronic spectroscopy of biexcitons in GaAs quantum wells. *Science* **2009**, *324*, 1169–1173.

42 Li, X.; Zhang, T.; Borca, C. N.; Cundiff, S. T. Many-body interactions in semiconductors probed by optical two-dimensional Fourier transform spectroscopy. *Phys. Rev. Lett.* **2006**, *96*, 057406.

43 Kim, Y. S.; Hochstrasser, R. M. Chemical exchange 2D IR of hydrogen-bond making and breaking. *Proc. Natl. Acad. Sci. U.S.A.* **2005**, *102*, 11185–11190.

44 Zheng, J.; Kwak, K.; Asbury, J.; Chen, X.; Piletic, I. R.; Fayer, M. D. Ultrafast dynamics of solute-solvent complexation observed by thermal equilibrium in real time. *Science* **2005**, *309*, 1338–1343.

45 Guo, C.; Shah, R. D.; Dukor, R. K.; Freedman, T. B.; Cao, X.; Nafie, L. A. Fourier transform vibrational circular dichroism from 800 to 10,000 cm^{-1}: Near-IR-VCD spectral standards for terpenes and related molecules. *Vib. Spectrosc.* **2006**, *42*, 254–272.

46 Dummer, D. J.; Kaplan, S. G.; Hanssen, L. M.; Pine, A. S.; Zong, Y. High-quality Brewster's angle polarizer for broadband infrared application. *Appl. Opt.* **1998**, *37*, 1194–1204.

47 Kwac, K.; Lee, C.; Jung, Y.; Han, J.; Kwak, K.; Zheng, J.; Fayer, M. D.; Cho, M. Phenol-benzene complexation dynamics: Quantum chemistry calculation, molecular dynamics simulations, and two dimensional IR spectroscopy. *J. Chem. Phys.* **2006**, *125*, 244508.

48 Brooks, B. R.; Bruccoleri, R. E.; Olafson, B. D.; States, D. J.; Swaminathan, S.; Karplus, M. CHARMM: A program for macromolecular energy, minimization, and dynamics calculations. *J. Comput. Chem.* **1983**, *4*, 187–217.

49 Guest, M. F.; Bush, I. J.; Van Dam, H. J. J.; Sherwood, P.; Thomas, J. M. H.; Van Lenthe, J. H.; Havenith, R. W. A.; Kendrick, J. The GAMESS-UK electronic structure package: algorithms, developments and applications. *Mol. Phys.* **2005**, *103*, 719–747.

50 Bridges, T. J.; Klüver, J. W. Dichroic calcite polarizers for the infrared. *Appl. Opt.* **1965**, *4*, 1121–1125.